Very large gold and silver sputtering yields induced by keV to MeV energy Au_n clusters (n = 1-13)

S. Bouneau, A. Brunelle, S. Della-Negra, J. Depauw, D. Jacquet, Y. Le Beyec, M. Pautrat, M. Fallavier, J.-C. Poizat, H.H. Andersen

Very large Gold and Silver Sputtering Yields Induced by keV to MeV Energy Au_n Gold Clusters (n = 1-13)

S. Bouneau[1], A. Brunelle[1*], S. Della-Negra[1], J. Depauw[1], D. Jacquet[1], Y. Le Beyec[1], M. Pautrat[1], M. Fallavier[2], J.C. Poizat[2] and H.H. Andersen[3]

[1] *Institut de Physique Nucléaire d'Orsay, UMR 8608, CNRS-IN2P3-Université Paris-Sud, 91406 Orsay Cedex, France*

[2] *Institut de Physique Nucléaire de Lyon, UMR 5822, CNRS-IN2P3-Université Claude Bernard 43 Boulevard du 11 novembre 1918, 69622 Villeurbanne Cedex, France*

[3] *Niels Bohr Institute, Ørsted Laboratory, Universitetsparken 5 DK-2100 Copenhagen Ø, Denmark*

PACS numbers : 79.20.Rf, 36.40.-c, 61.80.Lj, 68.49.Sf

Abstract

The total sputtering yields of gold and silver targets bombarded by Au_n (n = 1-13) clusters have been measured over a broad range of incident energy per atom (from 20 keV/atom to 5 MeV/atom). Large nonlinear effects in the sputtering yields were observed. For silver targets yield values as high as ~20 000 atoms per impact of Au_{13} at 1.2 MeV (92 keV/atom) were measured while only 45 atoms are emitted from the same target in the impact of single gold atoms at the same energy per atom. The sputtering yield variation with incident projectile energy per atom shows that maxima occur at 250 keV/atom for gold target and 150 keV/atom for silver target whatever the projectile size. In both cases the maxima of nuclear stopping power are at much larger energy per atom (700 keV for Au on Au and 550 keV for Au on Ag). Large surface deformations with crater and rim are observed by atomic force microscopy at the surface of cluster irradiated targets. Their number per unit area corresponds to the irradiation fluence. They demonstrate that a large amount of matter can be ejected per impact.

* Corresponding author. e-mail : brunelle@ipno.in2p3.fr

I. Introduction

Polyatomic projectiles bombarding solids give rise to various effects: crater formation, material modifications, secondary emission with yields (ions, neutrals) which are much larger than if induced by the same number of constituents arriving individually. Usually called nonlinear, these effects were first observed more than twenty years ago in sputtering.[1,2] Earlier data were summarized and discussed shortly before the present measuring series started.[3] Recently the total sputtering yield of a gold target bombarded by gold clusters Au_n (n = 1-5) was measured over a large incident energy range from 20 to 5000 keV per atom.[4] Sputtering yields as high as 3000 were found to be related to a dense energy deposition in the target through collisional nuclear processes. Unfortunately a few experimental yield values measured with Au_4 and Au_5 projectiles, between 100 and 200 keV/atom were overestimated and let us claim that the sputtering yield maxima were situated at a fixed total energy and not at the same energy per atom. The present paper is a continuation of the work of Ref. 4. Beams of large size gold clusters (up to Au_{13}) with higher intensities were used at both the Institut de Physique Nucléaire de Lyon (IPNL) and the Institut de Physique Nucléaire d'Orsay (IPNO) for systematic sputtering yield measurements from gold and silver surfaces.

II. Experimental

The gold cluster beams were mainly produced by a 2.5 MV Van de Graaff accelerator located at IPNL. This accelerator is equipped with a liquid metal ion source [5] installed in the high voltage terminal of the machine and produces beams of gold clusters accelerated to total energies from 300 keV to 1.4 MeV.[6] A magnet at the exit of the accelerator is used to select the chosen Au_n^+ cluster, with n from 1 to 13. As the magnet deflects the heavy gold clusters at a very small angle

only, a 6 m long beam tube has to be used to sufficiently separate the desired cluster from the others. The maximum bending power of the magnet permits to deviate Au_{13}^{+} ion beams having a total energy of 1.4 MeV at an angle of 3°. Above a total energy of 1.4 MeV, the cluster beams were delivered by the IPNO 15 MV tandem accelerator, which is also equipped with a liquid metal ion source in the high voltage terminal.[7] Data from Ref. 4 obtained from the Aramis accelerator (located at the C.S.N.S.M. laboratory at Orsay) have also been incorporated except the 4 points proved wrong by the present measuring series (see below).

The mass eroded from the target was measured with the quartz micro-balance method.[8] A schematic view of the experimental set-up is shown in Fig. 1. It has been completely rebuilt since the first experiments published in Ref. 4 and only the already described quartz micro-balance[†] is the same. Gold or silver is vapor deposited onto a standard quartz surface furnished by the micro-balance manufacturer. The thickness of the deposited metal is 10^4 Å, which is thick enough to stop the projectiles, whatever their energy, in the metal far before the quartz itself but is still thin enough not to disturb the quartz oscillations. The cluster beam passes through a 2.7 mm x 2.7 mm square aperture at the entrance of the experimental chamber. Its intensity is measured before each sputtering measurement with a Faraday cup located on the beam axis at the back of the chamber and equipped with secondary electron suppression. Upstream the Faraday cup the movable quartz micro-balance may be precisely positioned (± 0.2 mm) on the beam axis for the sputtering yield measurements. Because of the rapid decrease of the quartz gauge sensitivity with increasing distance between its centre and the beam axis (although the quartz diameter is 8 mm we have measured that 98% of its sensitive surface is situated within a 3 mm diameter; see also Ref. 9), it is very important to have both a precise and reproducible positioning of the quartz holder on the beam axis and a beam homogeneously irradiating the surface. The

[†] Model FTM5, Edwards, Manor Royal, Crawley, West Sussex, RH10, 2LW, UK

distance between the beam entrance aperture and the quartz is only 25 mm to ensure that possible misalignment of the beam gives rise to a negligible beam displacement on the quartz surface. It is possible at the IPNL Van de Graaff to rapidly sweep the beam horizontally and vertically with two sets of high voltage deflection plates located ~50 cm in front of the aperture to guarantee an homogeneous irradiation of the target whatever the beam profile. The beam currents varied under these conditions from several nA for Au_1 to 10 pA for Au_{13}. The minimum current accepted for the present experiments was 5 pA, as lower currents could not be measured reliably. Comparisons between experimental points measured with the same beam at different beam currents revealed that the intensity was underestimated by 20 to 40% below 5 pA, leading to a systematic overestimation of the sputtering yields for some experimental points in Ref. 4 (only 4 points out of 43). These experimental points (Au_4 at 100 and 187.5 keV/atom and Au_5 at 100 and 150 keV/atom) have been re-measured at the IPNL Van de Graaff in the present experiment.

The residual gas pressure in the experimental chamber and in the upstream beam line was always smaller than 10^{-4} Pa. The deflection plates shown in Fig. 1 were used to investigate break-up and charge exchange of the clusters through scattering on residual gas molecules during transmission through the 6 m beam tube. For that purpose a small air leak was introduced close to the entrance of the experimental chamber. An example is shown in Fig. 2, where the currents of Au_3^+ ions and the fragments Au_1^+ and Au_2^+ are plotted as a function of gas pressure between 4.10^{-5} and 8.10^{-4} Pa. A negligible fraction of less than 4% of the Au_3^+ ions was fragmented below 10^{-4} Pa. Therefore the residual gas pressure must be maintained below 10^{-4} Pa to avoid fragmentation. To test the possibility of neutralization, a sputtering yield measurement was performed during deflection of the charged beam for a time 10 times larger than usually necessary. No frequency variation of the quartz micro-balance was observed during that test experiment.

Our data contain measurements made with the old [4] and the present set-up and no systematic differences may be discerned. Within the experimental errors, estimated to be lower than 15%, our data are in agreement with previously published ones, obtained with gold,[10] lead [2] and bismuth [11] projectiles respectively onto gold targets.

Gold was first chosen in Ref. 4 in order to maximize the expected nonlinear effect and in order to avoid problems of target contamination by the incoming beam. The second surface chosen in the present experiments was silver. Although it has different mass, stopping power (for gold projectiles), density and surface binding energy than gold, the ratio of the nuclear stopping power over the surface binding energy was roughly the same as for gold.

III. Results and discussion

A. Sputtering yields as a function of projectile size and energy

Table I and Table II show the experimental sputtering yields divided by the number of constituents of the Au_n^+ (n = 1-13) gold cluster projectiles for gold and silver targets respectively. These values are presented in Fig. 3 as a function of the projectile energy per atom and without the error bars for clarity of the figure. This figure directly shows that sputtering yields per atom increase more rapidly at a given velocity than the number of constituents in the projectile, which means that strong nonlinear enhancements of the sputtering yield are induced by the impact of polyatomic projectiles. The maximum values obtained in the present experiments are 19 550 (± 1200) silver atoms sputtered per impact of 1200 keV Au_{13}, and 14 300 (± 1300) gold atoms per impact of 1400 keV Au_{13}. These sputtering yields are the highest ones ever obtained on metals. The silver sputtering yields are, for given cluster size and velocity, always larger than gold ones. This is not surprising if considering the gold surface binding energy (3.78 eV) which is larger than the silver one (3.04 eV).

For n = 1, yield variations as a function of energy present a maximum at roughly the same energy as the maximum of the nuclear stopping power at surface, ~700 keV and ~550 keV for gold onto gold and silver targets respectively (calculated with the SRIM2000 code).[12] For n values between 2 and 5, the yield curves have their maximum at the same projectile energy per atom, ~250 keV/atom for gold and ~150 keV/atom for silver, which are smaller than for the maximum of nuclear stopping power as given above. It was not possible for n larger than 5 to measure experimental values at energies per atom sufficiently high to reach the expected maximum yields, because of the limited energy range of the IPNL Van de Graaff as well as the limited beam intensity at the IPNO Tandem.

In order to highlight the strong increase of the experimental yields with increasing projectile size, Fig. 4 shows the variations of Y/n^2 as a function of the energy per atom. It is clear from this figure that above n = 2 (gold) and 3 (silver), all the sputtering yields roughly scale with n^2 and that the yields increase more rapidly than n^2 between n = 1 and 2 and between n = 2 and 3.

B. Target surface modifications and volume ejected

A Au_{11} cluster projectile having a total energy of 1.4 MeV (127 keV/atom) close to the maximum of the sputtering yield, ejects $12\,500 \pm 1700$ gold atoms from a gold target. This number corresponds to a volume of ~$2.1.10^5$ Å^3 (the density of gold is 19.3 g.cm^{-3}), which could be a cone with a depth h = 93 Å and base diameter D = h or a cylinder with a one monolayer height of 2.5 Å and a surface diameter of 330 Å. Atomic force microscopy (AFM) of a gold surface irradiated with these 127 keV/atom Au_{11} clusters was performed. The fluence was moderate, $1.61x10^{10}$ clusters.cm^{-2}, in order to have a negligible probability of crater overlapping. A perspective view of such an AFM image is shown in Fig. 5. The observed surface deformation has the shape of a crater surrounded by a rim. From the AB section in Fig. 5, one can estimate a crater diameter of 250 Å. It is larger than the one deduced from the sputtering yield but it is seen that a fraction of

the matter removed from the crater is re-deposited or pushed up around it. The crater depth cannot be deduced with certainty from an AFM measurement but on can nevertheless deduce an estimation of the cone depth from both the sputtered volume and the above crater diameter (Fig. 5). The obtained value of h~13 Å is finally intermediate between the two extreme cases mentioned above. A rough estimate of the number of craters per unit surface is in agreement within 20% with the irradiation fluence and it may further be seen that all the craters have very similar dimensions.

C. Sputtering yields as a function of nuclear stopping power

Fig. 6 shows total sputtering yields (not divided by n) as a function of the total nuclear stopping power at the surface (for the incident projectile energy per atom E/n). The electronic energy loss is not considered at all despite it amounts more than 20% of the total energy loss at the highest energies investigated. The stopping power, easy to calculate using SRIM tables, has been used. It is assumed that the nuclear stopping power of a Au_n^+ cluster is n times the nuclear stopping power of a single Au^+ ion at the same velocity. For a n constituent cluster projectile having a total energy E the notation is the following:

$$\left(\frac{dE}{dx}(n,E)\right)_{nuc} = n \times \left(\frac{dE}{dx}(1,E/n)\right)_{nuc} \qquad (1)$$

This assumption is in agreement with theoretical estimates [13] and supported by recent projected-range measurements.[14] Gold clusters Au_n (n = 1-3) at 10-40 keV/atom were implanted in Si, Al and Cu. The Si target was amorphous, the metal targets fine grained polycrystalline. Further, one set of measurements was performed with 44.3 keV/atom Au_1 and Au_7 in Si (amorphous). These range distributions were in all cases identical within their measuring accuracy.

For each cluster projectile size shown in Fig. 6 the total sputtering yields follow a line of slope 2 on a log-log presentation, as long as the energy remains below that of the yield maxima, indicating that in this region the yields are proportional to the square of the total nuclear stopping. Fig. 6 also

clearly shows that there is a region where the stopping still increases with energy, while the yields decrease with increasing energy. In this region the proportionality to $\left(\frac{dE}{dx}(n,E)\right)^2_{nuc}$ breaks down. These "hooks" in the curves demonstrate that there is no simple relation between the sputtering yields and the nuclear stopping power at surface. Similar curves have already been observed in the electronic stopping power regime[15] An effect of the projectile velocity appears, as slow projectiles induce larger yields than fast projectiles, although having same values of $\left(\frac{dE}{dx}(n,E)\right)_{nuc}$.

D. Comparisons with molecular dynamic simulations

Recent molecular dynamic (MD) simulations have been performed for gold sputtered under gold cluster bombardment. In Refs 16 and 17 gold clusters with energies per atom smaller than (or equal to) 16 keV/atom were used. The authors predict huge sputtering yields, depending strongly on cluster size and energy. The MD simulation pictures show that craters and crater rims are formed, as observed in the present work in AFM pictures. The simulations also demonstrate that a substantial fraction of the atoms excavated from the crater is redeposited to form a rim and that large clusters (chunks) are preferentially emitted around the craters. They also found a strong correlation between the crater size and the sputtering yield.

In Ref. 18 are presented simulations of Au_5 cluster impacts with a total energy of 800 keV. The authors predicted that a substantial fraction of the simulated impact produced no sputtering, while some individual sputtering events producing very large numbers of sputtered atoms contributed decisively to the total sputtering yield. The prediction of "super events" is in contradiction to the present AFM measurements (Fig. 5) in which no substantial fluctuation in the crater size is observed.

MD simulations accounting for electronic sputtering are presented in Refs. 19, 20 and 21. This work describes the energy relaxation mechanisms in solids independently of the energy deposition processes. It must, however, be noted that these simulations are performed for a condensed noble-gas target, and therefore comparisons with the present metal sputtering yields must be done with caution. The authors obtained a relation between the sputtering yield and a fraction of the electronically deposited energy, going into non-radiative de-excitations and contributing to sputtering. They concluded that the sputtering yield has a quadratic dependence on small stopping powers [$Y \propto (dE/dx)_{ele}^2$], and a linear dependence on large stopping powers [$Y \propto (dE/dx)_{ele}$]. In the present case of cluster bombardment and with the assumption of a nuclear stopping power proportional to the cluster size n, the sputtering yields should be proportional to n^2 and n in the two domains of energy deposition respectively. This predicted change could be connected in the present experiments to the fact that maxima of sputtering yields occur at velocities below those of the maxima of dE/dx, due to a maximum of energy deposition inside a cylindrical track.

E. Comparison with thermal spike models

The thermal spike theory of Sigmund and Claussen [22] was discussed in Ref. 4. In their model the sputtering yield is assumed to be the sum of the well established linear collision cascade yield [23] plus a contribution from a thermal spike induced surface evaporation. The calculated linear yield (which contains no free parameters) fits existing yield data for Au on Au and Ag very well at energies far above and below the maximum of the nuclear stopping power but underestimates the data in the region of the maxima of the sputtering yield and of nuclear stopping power.[3,10] For lighter particles and/or targets the linear yield is predicted very well indeed over the entire energy region.[24] The thermal spike in the model is assumed to be cylindrical, perpendicular to the surface and infinitely long in the version of the theory that we apply here. During evaporation from the

surface, the spike is cooled through heat conduction to the sides and the yield is obtained through an integration of the temperature-dependent evaporation over time. Sigmund and Claussen assumed in Ref. 22 that the spike evaporates at a rate small enough in order not to disturb the temperature profile. They also clearly pointed out the improvements needed by their model: (i) a more realistic spike geometry (Claussen [25] later worked out a theory based on a spherical spike model, but that model lead to unrealistic results), (ii) the cooling of the spike owing to energy loss by sputtering, (iii) fluctuations in energy deposition and (iv) crater formation. The only free parameter was the initial spike radius ρ_0. Sigmund and Claussen assumed $\langle r_0^2 \rangle$ to be of the order of the mean square lateral straggling of the collision cascade. Taking a constant cylindrical track radius $\langle r_0^2 \rangle = 240$ Å^2, they obtained a rather good agreement with the experimental values of Johar and Thompson.[11] All the experimental points of Ref. 11 were obtained at energies well below the maximum of the nuclear energy loss, where the sputtering yields are still relatively small in comparison to those obtained in the present work. To interpret the present results and then to obtain the necessary break in the proportionality between the sputtering yields and the nuclear stopping power, ρ_0 could be treated as a fitting parameter increasing with both cluster size and energy and a model that could predict these spike radii as a function of cluster size and velocity is needed within the framework of this spike model.

Other analytical theories are due to Bitensky,[26] Urbassek and Michl [27] and Jakas and Bringa.[28] Bitensky treats the influence of fluctuations on the onset of the spike. His theory is thus not relevant for large-cluster impacts, where we have full n^2-scaling and each event gives rise to a crater. Urbassek and Michl treats a gas flow model that may not be ruled out based on the present measurements. The model does, however, lead to a rather narrow angular distribution of the sputtered material which is in disagreement with recent results of Andersen et al.[29] Finally, Jakas and Bringa's model [28] is in its starting point close to that of Sigmund and Claussen [22] in the sense

that they start with a semi-infinite cylinder with a constant high temperature proportional to dE/dx. As suggested by the simulations of Bringa et al [19,20,21] they assume the sputtered material to be expelled by a pressure pulse, which also dissipates energy radially from the spike, where Sigmund and Claussen assumed heat conduction. Jakas and Bringa cannot reproduce the dE/dx proportional results of Bringa et al, but find a faster rise of the yield with dE/dx. Unfortunately, we cannot extract numerical values for the spike radii, as we could from the Sigmund-Claussen theory. They might, in case we could, also have been meaningless, as the noble-gas interaction potential used by Jakas and Bringa clearly is not well suited for our metal targets.

As in Ref. 20 where it is shown that radial energy transport limits the sputtering yield, recent studies of Jakas and Bringa [28] include the transport of mass, a realistic heat capacity and the heat of melting in an extended version of the standard thermal spike theory of sputtering.[22] Although their calculations account for much lower deposited energy values than in the present case, they concluded that at large deposited energies the thermal pressure in the hot core of the spike gives rise to an elastic wave, which expands laterally and cools the spike, lowering the sputtering yield. A process of that kind could explain why the experimental sputtering yield maxima are reached at energy per atom lower than for the maximum nuclear stopping power.

IV. Conclusion

Following a series of previous measurements [4] on sputtering of Au targets with limited size of Au_n clusters (n = 1-5), new measurements over a broad projectile energy interval have been pursued with large cluster size (up to n = 13) and with both gold and silver targets. It is observed that for clusters with $n \geq 3$ all the sputtering yields are proportional to the square of the number of constituents and have their maxima at the same energy per atom which is much smaller than the energy of the maximum of the nuclear stopping power.

The sputtering yield values that have been measured are the largest ever observed with metallic targets and could not be predicted by theoretical models in the energy range investigated. The thermal spike model may be used to estimate the sputtering yield provided the variation of the track radius parameter values with energy and cluster size is known.

Hydrodynamic effects are not considered in the spike model but it is likely that they play a role as shown in molecular dynamic simulations that we have shortly discussed. At high energies such simulations with large size clusters cannot practically be obtained with reasonable statistics. The simulations could explain however (at relatively low impact energies) the formation of craters and rims as observed at the surface of gold layers.

In the future, the size of the projectiles could be increased to a point where an important fraction of the energy is released through sputtering processes and it would be also interesting to explore the sputtering limit in terms of ejected matter per impact of large object. Beams of gold clusters containing up to 100 atoms were already accelerated to several tens of keV/atom. Large intact clusters and/or chunks of matter will certainly be emitted in the bombardment of solids with these beams. This probably occurs already with the beams of Au_n used in this work and cluster emission should be considered in models. Measurements of the mass distribution of the sputtered species with a post-ionization method should thus be performed. Large enhancements of secondary ion emission yields were previously measured with gold clusters in the same incident energy range but with different types of materials.[30] The highest ion emission yields were also observed at much lower energy per atom than the expected maxima of the nuclear stopping. This behaviour seems to be a general trend in large cluster induced secondary emission.

Acknowledgements

Technical support during the experiments by Y. Champelovier (IPNL Van de Graaff accelerator) and by the IPN-Orsay Tandem accelerator group is gratefully acknowledged. We also thank J.C. Girard from the University of Poitiers who performed the AFM measurements. One author (H.H.A.) thanks the Danish National Science Research Council (SNF) for grants which allowed his participation in the experiments.

Figure captions:

Fig. 1: Schematic view of the sputtering yield measurement set-up.

Fig. 2: Beam intensities measured with a Faraday cup for Au_3^+ ions and the fragment ions Au_2^+ and Au_1^+, at 302 keV/atom, as a function of residual gas pressure. The solid lines are guides for the eye.

Fig. 3: Gold and Silver sputtering yields per atom Y/n, as a function of the energy per atom of the Au_n (n = 1-13) gold cluster projectiles. The solid lines are guides for the eye. Symbols used correspond to following values of n:

+ 1 × 2 □ 3 △ 4 ● 5 ○ 7 ▼ 9 ■ 11 ▲ 13

Fig. 4: Gold and silver sputtering yields divided by n^2, as a function of the energy per atom of the Au_n (n = 1-13) gold cluster projectiles. The dashed lines are guides for the eye. Symbols correspond to Fig. 3.

Fig. 5: Atomic force microscope image (perspective view) of a gold surface (area = 5000 Å x 5000 Å) irradiated with $1.61.10^{10}/cm^2$ Au_{11} ions having an energy of 1.4 MeV (127 keV/atom).

Fig. 6: Gold and silver total sputtering yields Y, as a function of the tabulated [12] projectile nuclear stopping power $n\times\left(\frac{dE}{dx}(1,E/n)\right)_{nuc}$ and for Au_n (n = 1-13) cluster projectiles. Symbols correspond to Fig. 3. solid lines are guides for the eye.

Table I : Gold sputtering yields per atom measured for different gold cluster projectiles

Table II : Silver sputtering yields per atom measured for different gold cluster projectiles

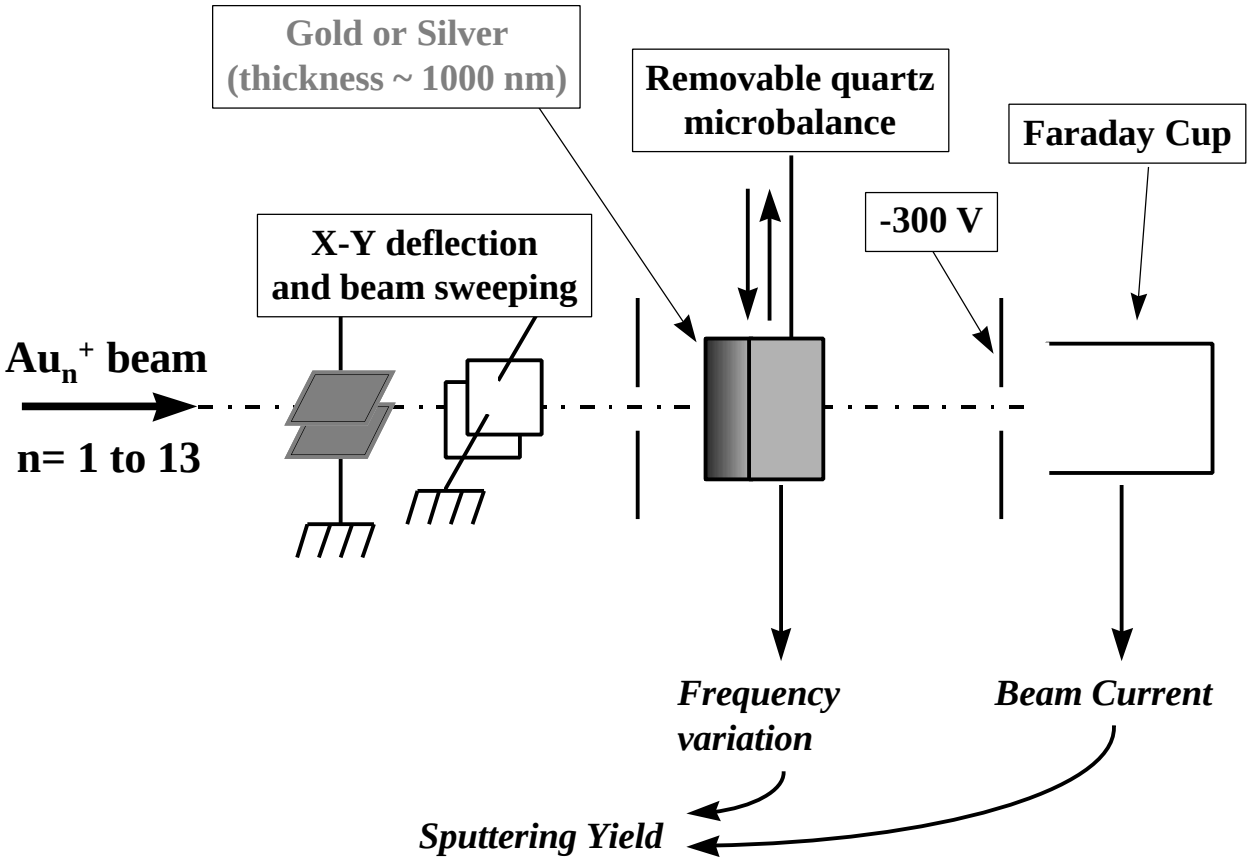
Gold or Silver
(thickness ~ 1000 nm)
Removable quartz
microbalance
Faraday Cup
-300 V
X-Y deflection
and beam sweeping
Au$_n^+$ beam
n= 1 to 13
Frequency
variation
Beam Current
Sputtering Yield

Fig. 1

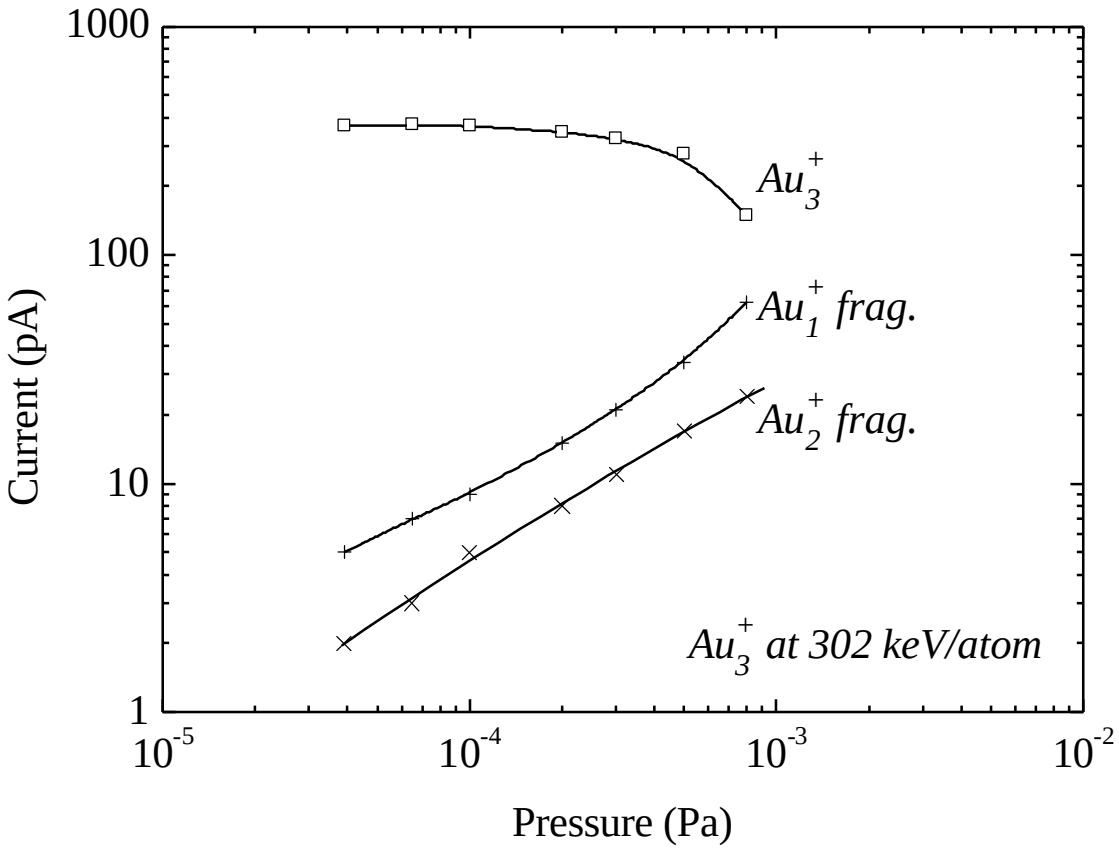
1000
100
10
1
Current (pA)
10^{-5}
10^{-4}
10^{-3}
10^{-2}
Pressure (Pa)
Au_3^+
Au_1^+ frag.
Au_2^+ frag.
Au_3^+ at 302 keV/atom

Fig. 2

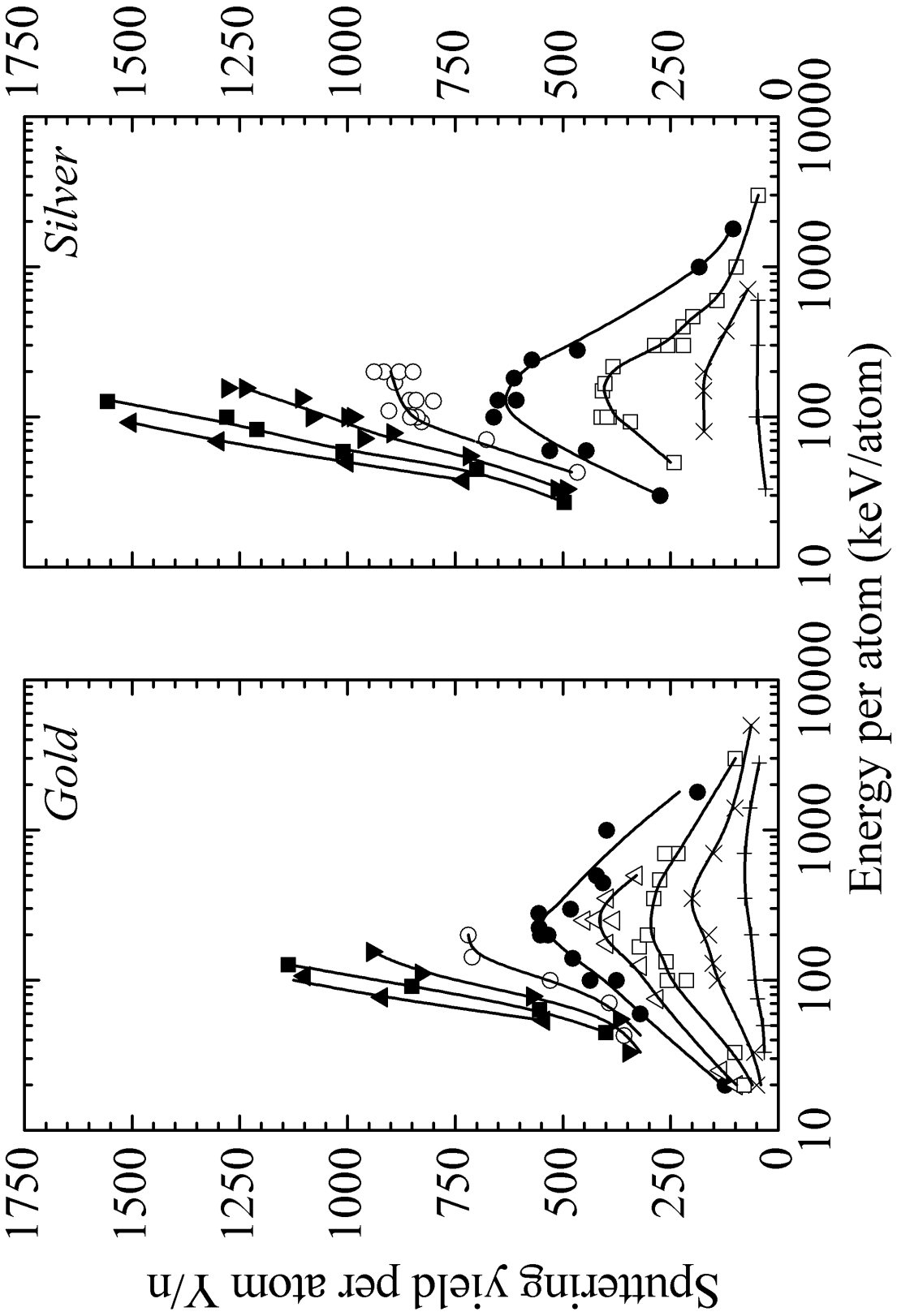
Sputtering yield per atom Y/n
Energy per atom (keV/atom)
Gold
Silver
0
250
500
750
1000
1250
1500
1750
10
100
1000
10000

Fig. 3

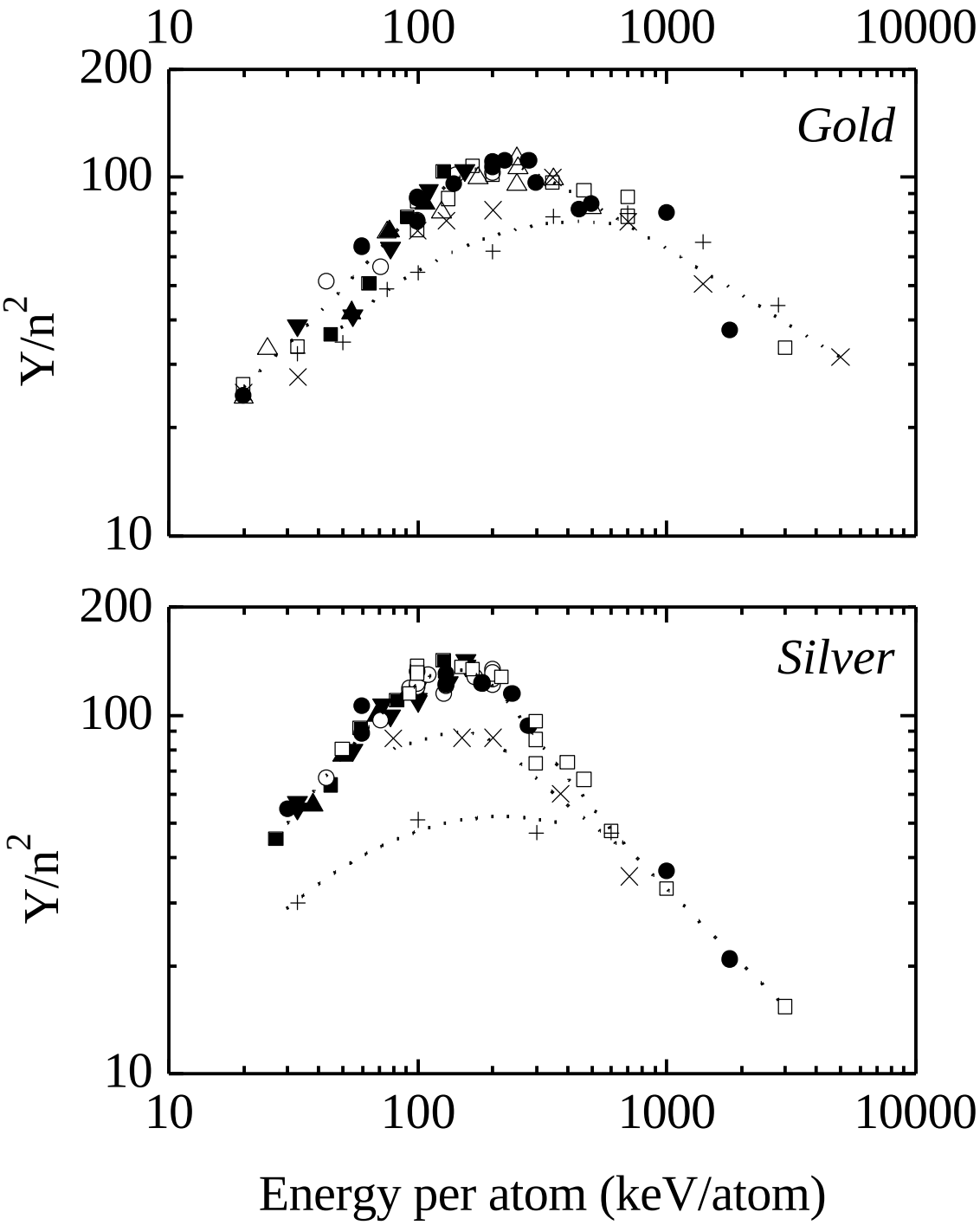
10
100
1000
10000
200
100
10
Gold
Y/n2
Silver
Energy per atom (keV/atom)

Fig. 4

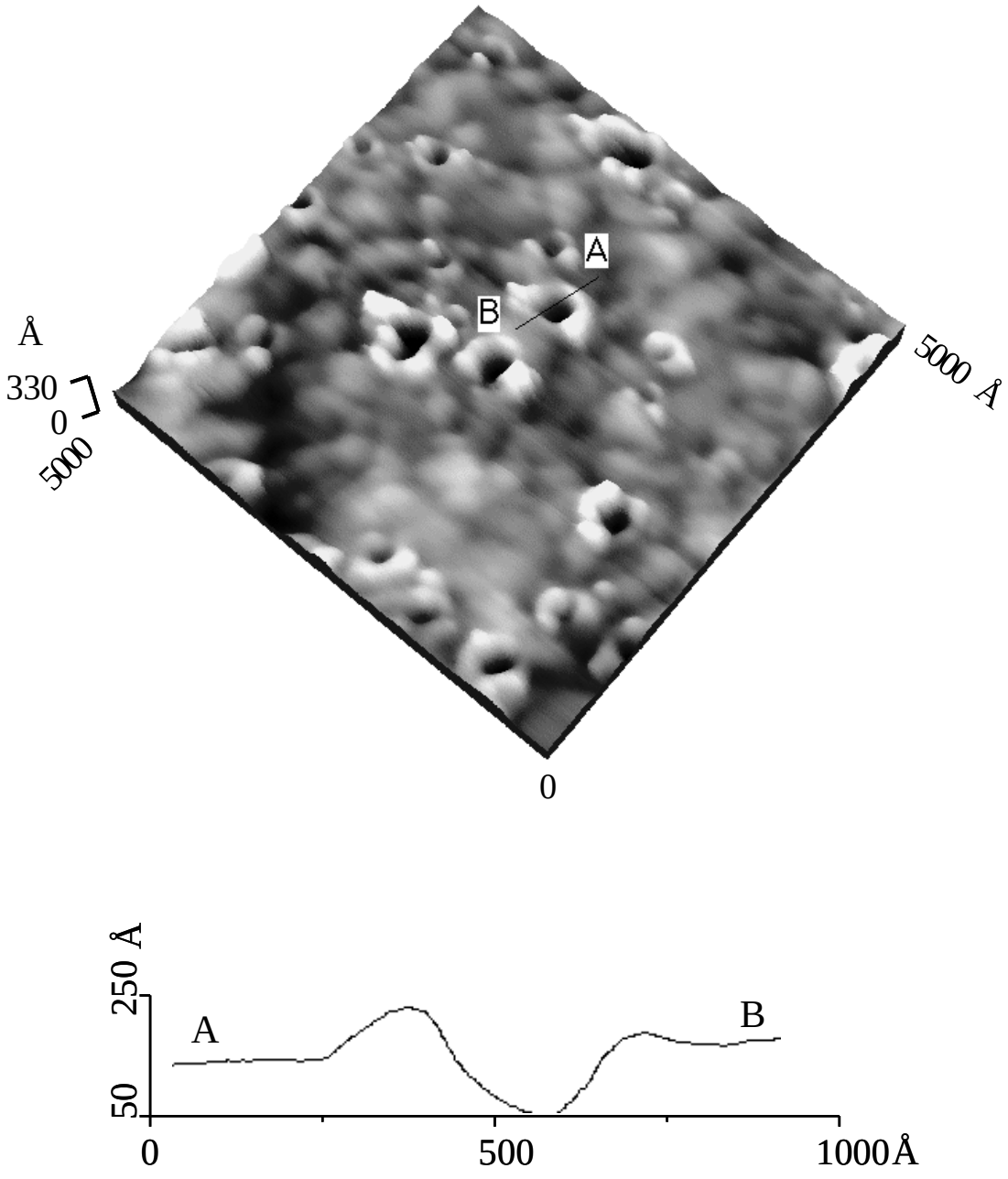

Fig. 5

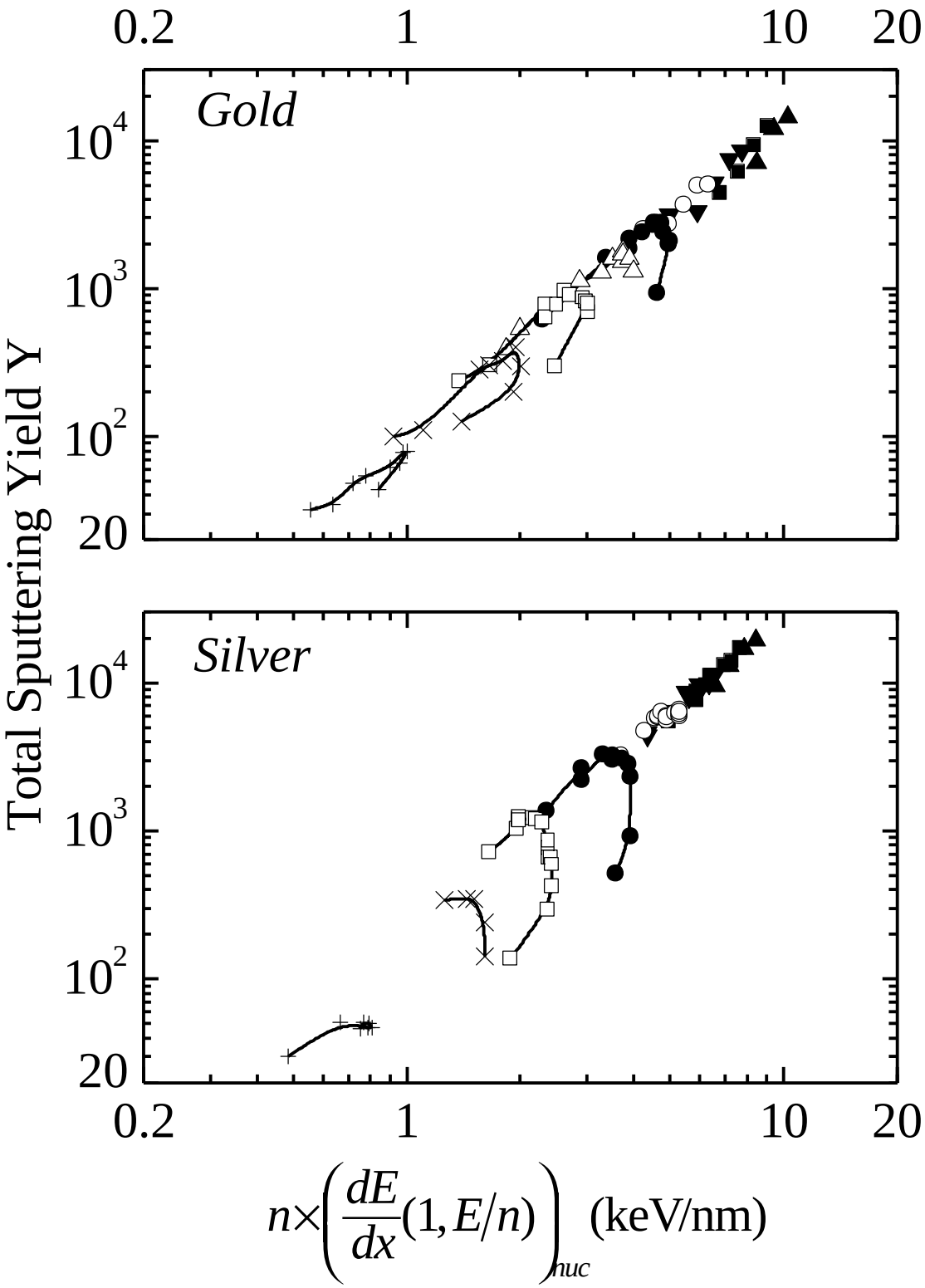
0.2
1
10
20
Gold
10^4
10^3
10^2
20
Silver
Total Sputtering Yield Y
$n\times\left(\frac{dE}{dx}(1,E/n)\right)_{nuc}$ (keV/nm)

Fig. 6

Table I : Gold sputtering yields per atom measured for different gold cluster projectiles

Projectile	Incident energy per atom (keV/atom)	Sputtering yield per atom Y/n
Au_1	33	32 ± 2
	50	34.5 ± 4
	75	49 ± 6
	100	54 ± 5
	200	62 ± 6.5
	350	78 ± 6
	700	79 ± 7
	1400	66 ± 5.5
	2800	44 ± 3.5
Au_2	20	50 ± 4
	33	55 ± 5.5
	100	142 ± 14.5
	130	152 ± 15
	200	162 ± 18
	350	200 ± 22.5
	700	150 ± 18
	1400	101 ± 12
	5000	63 ± 5
Au_3	20	79 ± 5.5
	33	101 ± 9.7
	100	235 ± 25
	133	261 ± 26
	167	322 ± 18
	200	303 ± 17
	350	289 ± 15
	468	275 ± 17
	700	248 ± 16
	3000	100 ± 6
Au_4	20	97 ± 8
	25	133 ± 11
	75	281 ± 30
	125	319 ± 29
	175	397 ± 31
	250	418 ± 39
	351	396 ± 57
	500	329 ± 34

Projectile	Incident energy per atom (keV/atom)	Sputtering yield per atom Y/n
Au_5	20	123 ± 16
	60	320 ± 32
	100	406 ± 28
	140	477 ± 42
	200	543 ± 40
	224	555 ± 136
	280	556 ± 42
	299	482 ± 55
	446	407 ± 52
	500	422 ± 73
	1000	398 ± 32
	1800	187 ± 20
Au_7	43	358 ± 77
	71	392 ± 29
	100	529 ± 41
	143	710 ± 82
	200	719 ± 55
Au_9	33	348 ± 21
	55	370 ± 38
	78	572 ± 97
	111	830 ± 80
	155	943 ± 103
Au_{11}	45	400 ± 39
	64	554 ± 43
	91	850 ± 62
	127	1140 ± 160
Au_{13}	54	544 ± 49
	77	920 ± 90
	107	1100 ± 102

Table II : Silver sputtering yields per atom measured for different gold cluster projectiles

Projectile	Incident energy per atom (keV/atom)	Sputtering yield per atom Y/n
Au_1	33	30 ± 2
	100	51 ± 3
	300	47 ± 3
	600	47 ± 5
Au_2	80	172 ± 7.5
	150	173 ± 9.6
	200	173 ± 5.2
	375	121 ± 2.7
	710	71 ± 2.5
Au_3	50	241 ± 13.5
	93	343 ± 20
	100	400 ± 22
	150	408 ± 26
	167	402 ± 24
	217	383 ± 24
	300	254 ± 16
	400	221 ± 10
	467	198 ± 12
	600	142 ± 12
	1000	98 ± 6
	3000	46 ± 2.5
Au_5	30	274 ± 17
	60	488 ± 25
	100	660 ± 41
	130	629 ± 35
	182	613 ± 38
	240	572 ± 29
	280	466 ± 30
	1000	183 ± 14
	1800	104 ± 11.5

Projectile	Incident energy per atom (keV/atom)	Sputtering yield per atom Y/n
Au_7	43	466 ± 28
	71	677 ± 43
	93	828 ± 73
	100	846 ± 50
	110	904 ± 93
	128	800 ± 47
	130	848 ± 70
	171	890 ± 35
	200	895 ± 60
Au_9	33	504 ± 30
	55	718 ± 47
	72	963 ± 80
	78	896 ± 51
	100	1023 ± 72
	133	1108 ± 67
	156	1260 ± 73
Au_{11}	27	497 ± 56
	45	700 ± 50
	59	1010 ± 77
	82.7	1210 ± 152
	100	1280 ± 64
	127	1560 ± 90
Au_{13}	38	731 ± 50
	50	1000 ± 73
	69	1300 ± 156
	92	1500 ± 95

References

[1] H.H. Andersen, H.L. Bay, J. Appl. Phys. **45**, 953 (1974).

[2] H.H. Andersen, H.L. Bay, J. Appl. Phys. **46**, 2416 (1975).

[3] H.H. Andersen, Mat. Fys. Medd. Dan. Vid. Selsk, **43**, 127 (1993).

[4] H.H. Andersen, A. Brunelle, S. Della-Negra, J. Depauw, D. Jacquet, Y. Le Beyec, J. Chaumont, H. Bernas, Phys. Rev. Lett. **80**, 5433 (1998).

[5] M. Benguerba, A. Brunelle, S. Della-Negra, J. Depauw, H. Joret, Y. Le Beyec, M.G. Blain, E.A. Schweikert, G. Ben Assayag, P. Sudraud, Nucl. Instrum. Methods. Phys. Res., Sect. B **62**, 8 (1991).

[6] M. Fallavier, Y. Champelovier, M. Ferrari, R. Kirsch, J.C. Poizat, J. Remillieux, J.P. Thomas, B. Canut, S.M.M. Ramos, P. Thévenard, S. Della-Negra, J.P. Mouffron, P. Nicol, Eur. Phys. J. D **9**, 529 (1999).

[7] S. Della-Negra, A. Brunelle, Y. Le Beyec, J.M. Curaudeau, J.P. Mouffron, B. Waast, P. Håkansson, B.U.R. Sundqvist, and E.S. Parilis, Nucl. Instrum. Methods. Phys. Res., Sect. B **74**, 453 (1993).

[8] H.H. Andersen and H.L. Bay, Radiat. Eff. **13**, 67 (1972).

[9] A. Oliva-Florio, R.A. Baragiola, M.M. Jakas, E.V. Alonso, J. Ferron, Phys. Rev. B **35**, 2198 (1987).

[10] H.L. Bay, H.H. Andersen, W.O. Hofer, O. Nielsen, Nucl. Instrum. Methods. Phys. Res. **132**, 301 (1976)

[11] S.S. Johar, D.A. Thompson, Surf. Sci. **90**, 319 (1979)

[12] J.F. Ziegler, J.P. Biersack, H. Littmark, The Stopping and Ranges of Ions in Solids, Pergamon Press, New York, 1985.

[13] V.I. Shulga and P. Sigmund, Nucl. Instrum. Methods. Phys. Res., Sect. B **47**, 236 (1990).

[14] H.H. Andersen, A. Johansen, M. Olsen and V. Tuboltsev, to be published.

[15] P. Dück, W. Treu, H. Fröhlich, W. Galster, H. Voit, Surf. Sci. **95**, 603 (1980)

[16] Th.J. Colla, H.M. Urbassek, Nucl. Instrum. Methods. Phys. Res., Sect. B, **164-165**, 687 (2000).

[17] Th.J. Colla, R. Aderjan, R. Kissel, H.M. Urbassek, Phys. Rev. B **62**, 8487 (2000).

[18] M.H. Shapiro, T.A. Tombrello, Nucl. Instrum. Methods. Phys. Res., Sect. B **152**, 221 (1999).

[19] E.M. Bringa, R.E. Johnson, Nucl. Instrum. Methods. Phys. Res., Sect. B **143**, 513 (1998).

[20] E.M. Bringa, R.E. Johnson, L. Dutkiewicz,
Nucl. Instrum. Methods. Phys. Res., Sect. B **152**, 267 (1999).

[21] E.M. Bringa, M.M. Jakas, R.E. Johnson,
Nucl. Instrum. Methods. Phys. Res., Sect. B, **164-165**, 762 (2000).

[22] P. Sigmund, C. Claussen, J. Appl. Phys. **52**, 990 (1981).

[23] P. Sigmund, Phys. Rev. **184**, 383 (1969); **187** 768 (1969).

[24] H.H. Andersen and H.L. Bay, in "Sputtering by Particle Bombardment I,
R. Behrisch, editor, Springer-Verlag Berlin Heidelberg **47**, 145 (1981).

[25] C. Claussen, Nucl. Instrum. Methods. Phys. Res., **194**, 567 (1982).

[26] I.S. Bitensky, Nucl. Instrum. Methods. Phys. Res., Sect. B, **83**, 110 (1993).

[27] H.M. Urbassek and J. Michl, Nucl. Instrum. Methods. Phys. Res., Sect. B, **22**, 480 (1987).

[28] M.M. Jakas, E.M. Bringa, Phys. Rev. B **62**, 824 (2000).

[29] H.H. Andersen, A. Johansen and V.S. Touboltsev,
Nucl. Instrum. Methods. Phys. Res., Sect. B, **164-165**, 727 (2000).

[30] A. Brunelle, S. Della-Negra, J. Depauw, D. Jacquet, Y. Le Beyec, M. Pautrat, K. Baudin,
H.H. Andersen, Phys. Rev. A **63**, 22902 (2001).